Supporting Information

Hanske et al. 10.1073/pnas.1112312108

SI Materials and Methods

Site-Directed Mutagenesis, Protein Expression, and Purification. Single Cys residues were introduced by point mutations of the pBTR plasmid (1) using the QuickChange kit (Stratagene). The template was digested with DpnI (New England Biolabs), and the resulting plasmids were transformed into XL1-Blue cells (Agilent). DNA was extracted using a Miniprep Kit (Qiagen) and sequenced at the Molecular Biology and Proteomics Core Facility (Dartmouth College).

The cyt *c* mutant plasmid was transformed into *Escherichia coli* BL21 Star cells (Invitrogen) and plated on LB agar with 100 μg/mL of ampicillin. A single colony was selected and grown in 7 mL of Terrific Broth (TB) medium containing 100 μg/mL of ampicillin for 6–8 h. This culture was used to inoculate six 2.8-liter flasks of TB medium containing 100 μg/mL of ampicillin (one liter of medium in each flask, 1 mL of starting culture/liter of medium to inoculate). The large-scale cultures were grown at 37 °C for 18–22 h until centrifuged 1 mL samples from each flask displayed bright fuchsia pellets.

Cells were harvested by centrifugation and resuspended in 30 mL of 100 mM Tris-HCl pH 8.0 buffer. Crystalline lysozyme (10 mg/g wet cell paste) was dissolved in the cell suspension, followed by freezing overnight at −80 °C. Frozen cell suspension was defrosted in room temperature water, after which protease inhibitor (1 mM PMSF) and DNase (0.3 mL of 10 mg/mL stock solution per 100 mL of cell suspension) were added to the cell suspension. The thawed cell suspension was French pressed at 4 °C in 35–45 mL aliquots. The pressed cells were centrifuged at 16,000 rpm (Beckman JA-25.50 rotor) for one hour and the supernatant was collected.

To purify the crude protein, 351 g/L of ammonium sulfate was slowly added to the supernatant while stirring. The resulting solution was centrifuged at 13,500 rpm (Beckman JA-14 rotor) for 20 min to remove the ammonium sulfate precipitate. The supernatant was dialyzed overnight against distilled water using the 3,500 Molecular Weight Cut-Off SnakeSkin Dialysis Tubing (ThermoFisher). Protein was concentrated to a volume of approximately 50 mL using an Amicon concentrator and dialyzed overnight again in 10 mM NaPi containing 1 mM DTT at pH 7.4. Purification was continued with a fast protein liquid chromatography system (GE Healthcare FPLC) with a HiLoad 26/10 SP Sepharose HP column. The column was equilibrated with 10 mM NaPi containing 1 mM DTT at pH 7.4 and the protein eluted with a linear gradient of NaCl from 0 to 0.4 M in the same buffer.

Preparation of Lipid Vesicles. Chloroform stocks of 1,2-dioleoyl-*sn*-glycero-3-phosphocholine (DOPC) and 1,1′,2,2′-tetraoleoyl-cardiolipin (TOCL) (1:1 molar ratio), both from Avanti Polar lipids, were dried under a stream of nitrogen gas and resuspended in a 25 mM Hepes buffer pH 7.4 to a final lipid concentration of 3.3 mM [cmc of CL vesicles is approximately 1 μM (2)]. Small unilamellar vesicles were prepared by sonication (30 s on/30 s off for 30 min) of the lipid solution with a Branson Ultrasonics microtip connected to a Fisher Scientific Sonic Dismembrator Model 500. The resulting clear solution was passed through a 0.22 μm filter to remove titanium dust. Dynamic light scattering measurements, using a Malvern Instruments Zetasizer Nano ZS, indicated that the vesicles in our experiments had average radii of 35–43 nm. Addition of 5 μM cyt *c* and ≤1 M NaCl had minor effects on the size distribution of the vesicles (a maximum of 7–10% increase in the average size with 1 M salt). Liposome solutions were stored at room temperature and used within 24 h of preparation. No evidence of vesicle aggregation was detected within this time period.

Data Analysis of TR-FRET. Data analysis of the TR-FRET was done in MATLAB (MathWorks) by performing the numerical inversion of a Laplace transform $I(t) = \Sigma_k P(k) \exp(-kt)$ on the basis set of logarithmically spaced rate constants k using regularization methods that impose additional constraints on the properties of the distribution of rate constants $P(k)$ (3, 4). Information theory suggests that the least biased solution to the inversion problem minimizes the sum of the squared deviations (χ^2) and maximizes the breadth of $P(k)$ (5). Maximum entropy and MATLAB LSQNONNEG ($P(k) \geq 0, \forall\, k$) algorithms have been described in detail (3, 4). In addition, simultaneous minimization of the squared deviations χ^2 between the calculated and experimental intensities $I(t)$ and the weighted sum of the squared gradient of the $P(k)$ function (an algorithm developed by Jay R. Winkler) was used as an alternative approach to broaden the LSQNONNEG solution. The three-point gradient for $P(k_i)$ gradient was calculated from the polynomial coefficients by fitting the three points, $[P(k_{i-1}), P(k_i), P(k_{i+1})]$ to a second-order polynomial. Fitting of the data with these regularization methods provided stable and reproducible numerical inversions of the kinetics data, yielding upper limits for the widths of $P(k)$ consistent with the experimental data.

A coordinate transformation using the Förster relation (Eq. **S1**) was used to convert the $P(k)$ distributions to the distributions of the ***D-A*** distances $P(r)$. In Eq. **S1**, R_0 is the Förster critical distance. The fluorescence decay rate constant of the unquenched dansyl (Dns) group, $k_0 = 9.8 \times 10^7\ s^{-1}$, was determined with *N*-acetyl Cys-Dns model compound and was not affected by addition of CL liposomes.

$$k = k_0\left(1 + \left(\frac{R_0}{r}\right)^6\right). \qquad \textbf{[S1]}$$

The resolution limit of rate constants k and thus ***D-A*** distances r depends on the signal-to-noise levels, S/N in experiments measuring multiexponential decays (5). For our studies, S/N levels were ∼500 giving the relative precision in the r-values of 10–15% for $r < R_0$. The uncertainty increases significantly at longer distances and at $r > 1.5 \times R_0$, energy transfer rate constants and ***D-A*** distances cannot be determined reliably. However, even with these uncertainties, the large r differences for compact and extended conformations result in clear differences in rates, visible even in raw experimental decays without additional analysis of the data.

Our S/N levels as well as analysis of blank samples suggest a ∼3% detection limit for extended conformers in the ensemble. The limit is important to consider in the analysis of catalytic reactions. Fortunately, peroxidase activity is a sensitive indicator of unfolded conformations that may not be otherwise visible by spectroscopic means (6). Therefore, we have combined activity and TR-FRET assays to describe the behavior of the entire cyt *c* ensemble and observed meaningful correlations between the two sets of experimental results.

Orientation Factor κ^2 and Critical Distance R_0. Calculations of ***D-A*** distances were based on the isotropic κ^2 value of 2/3. Similarly to Dns variants in yeast cyt *c* (7), time-resolved anisotropy data $r(t)$ (Table S3) suggest that this assumption is justified for all unfolded and folded variants in this study. The decays $r(t)$ can be well fit to two correlation times ϕ (Eq. **S2**) with a prominent contribution of the ϕ_{fast} correlation time that likely corresponds

to tether-arm, side chain, and small-scale peptidyl segmental motion (8). The Dns fluorescence is almost fully depolarized within the fluorophore lifetime, suggesting that the fluorophore does not adopt a single orientation with respect to the heme group.

$$r(t) = a_{\text{fast}} \exp(-t/\phi_{\text{fast}}) + a_{\text{slow}} \exp(-t/\phi_{\text{slow}}) + r_{\infty}. \qquad \textbf{[S2]}$$

Binding to CL vesicles does slow down the depolarization process of Dns fluorescence; however, the limiting values r_{∞} are relatively small ($\leq$25% of the $r(t)$ signal amplitude). Similar magnitudes of r_{∞} values for the four variants suggest that the uniform treatment of κ^2 across the series is reasonable. The nonzero r_{∞} values likely arise from tumbling dynamics of the vesicle-bound protein, but fast local and global depolarization pathways of the Dns fluorescence still remain. These faster processes, together with small shifts in λ_{max} upon CL binding in all four variants, suggest that likely the Dns probe in none of them is fully trapped to dramatically limit the range of possible orientations between the transition dipoles of ***D*** and ***A***. In addition, recent molecular dynamics simulations have indicated that the lipid environment has a minimal effect on the conformational space of the Dns fluorophore in labeled proteins, suggesting that this probe can move relatively unhindered within the membranes (9). Furthermore, degenerate *x*- and *y*- polarized absorption bands in the heme acceptor imply that the transitional moment of this group may have any orientation within the plane of the porphyrin (10, 11).

Because R_0 is determined by the sixth root of κ^2, its value is not very sensitive to the uncertainties in κ^2. Even under the scenario when the Dns and heme probes transition dipole moments are collinear and κ^2 is at the theoretical maximum of 4, the R_0 value differs by less than 40% from that calculated with the isotropic value $\kappa^2 = 2/3$; we conservatively examine this source of error in the discussion of fast rates. Despite the uncertainty of the exact value of the κ^2 parameter, the conclusions of this study are not affected. The multiphasic nature of the FRET kinetics clearly points to different types of polypeptide structures in the ensemble and the existence of structures that strongly resemble those for the fully unfolded state of the protein.

The Förster distance R_0 for the Dns-heme pair calculated with $\kappa^2 = 2/3$ is 39 Å, which allows distances between 12 and 59 Å to be accurately measured (7). Changes in the heme absorption spectra due to alteration in the spin and ligation states introduce minimal changes (<1 Å) in the R_0 value.

Cyt *c*-Liposome Binding Assays. The following assay was used to compare the similarities in binding of labeled cyt *c* variants and the wild-type horse heart protein to TOCL/DOPC liposomes. In contrast to absorption and fluorescence measurements, this assay is not complicated by protein unfolding. Although this measurement examines nonequilibrium protein concentrations, it is done under identical conditions and provides an important comparison of CL binding for the variants.

To ensure uniform pelleting, TOCL/DOPC liposomes were prepared by extrusion through a 0.1 μm SPI-Pore membrane (11 cycles). Solutions containing different amounts of liposomes in a 25 mM Hepes buffer at pH 7.4 and identical concentrations of protein were prepared. Samples were mixed by pipetting and incubated 30 min prior to centrifugation. The samples were centrifuged for 60 min using a Beckman Airfuge tabletop ultracentrifuge equipped with a Beckman A-11 rotor. The centrifuge was run at 160,000 × *g* using compressed nitrogen. After completion of each run, the supernatant was immediately removed and its absorption spectrum measured. Bound (pelleted) protein was calculated as total minus free. All Dns-labeled protein samples were protected from light with foil during incubation and centrifugation. Long incubation times, particularly under oxygen-free conditions in the centrifuge, resulted in a small amount (<20%) of cyt *c* being reduced. The protein concentrations in the experiments were between 3.6 and 4.9 μM.

1. Patel CN, Lind MC, Pielak GJ (2001) Characterization of horse cytochrome *c* expressed in *Escherichia coli*. *Protein Expr Purif* 22:220–224.
2. Sinibaldi F, et al. (2008) Insights into cytochrome *c*-cardiolipin interaction. Role played by ionic strength. *Biochemistry* 47:6928–6935.
3. Pletneva EV, Gray HB, Winkler JR (2005) Nature of the cytochrome *c* molten globule. *J Am Chem Soc* 127:15370–15371.
4. Zhang X, et al. (2011) Direct visualization reveals dynamics of a transient intermediate during protein assembly. *Proc Natl Acad of Sci USA* 108:6450–6455.
5. Istratov AD, Vyvenko OF (1999) Exponential analysis in physical phenomena. *Rev Sci Instrum* 70:1233–1257.
6. Diederix RE, Ubbink M, Canters GW (2002) Peroxidase activity as a tool for studying the folding of *c*-type cytochromes. *Biochemistry* 41:13067–13077.
7. Pletneva EV, Gray HB, Winkler JR (2005) Many faces of the unfolded state: Conformational heterogeneity in denatured yeast cytochrome *c*. *J Mol Biol* 345:855–867.
8. Shi J, Tai K, McCammon JA, Taylor P, Johnson DA (2003) Nanosecond dynamics of the mouse acetylcholineesterase Cys^{69}-Cys^{96} omega loop. *J Biol Chem* 278:30905–30911.
9. Vos WL, Schor M, Baumgaertner A, Tieleman DP, Hemminga MA (2010) Molecular dynamics simulations reveal that AEDANS is an inert fluorescent probe for the study of membrane proteins. *Eur Biophys J* 39:229–239.
10. Eaton WA, Hochstrasser RM (1967) Electronic spectrum of single crystals of ferricytochrome-*c*. *J Chem Phys* 46:2533–2539.
11. Domanov YA, Molotkovsky JG, Gorbenko GP (2005) Coverage-dependent changes of cytochrome *c* transverse location in phospholipid membranes revealed by FRET. *Biochim Biophys Acta* 1716:49–58.

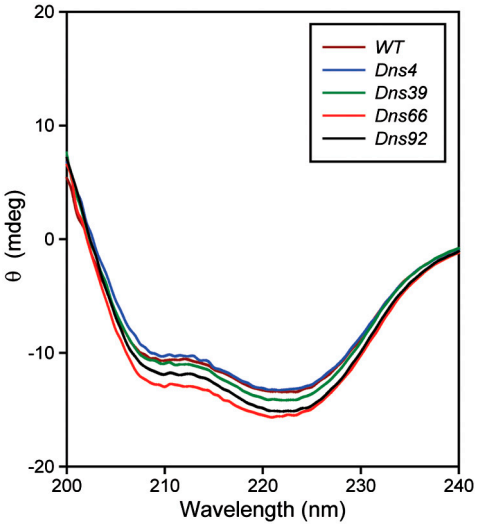

Fig. S1. Far-UV CD spectra of the wild-type and Dns-labeled cyt *c* variants in a 100 mM sodium phosphate buffer at pH 7.4 and 22 °C: [cyt *c*] = 10.0 μM, *l* = 0.1 cm.

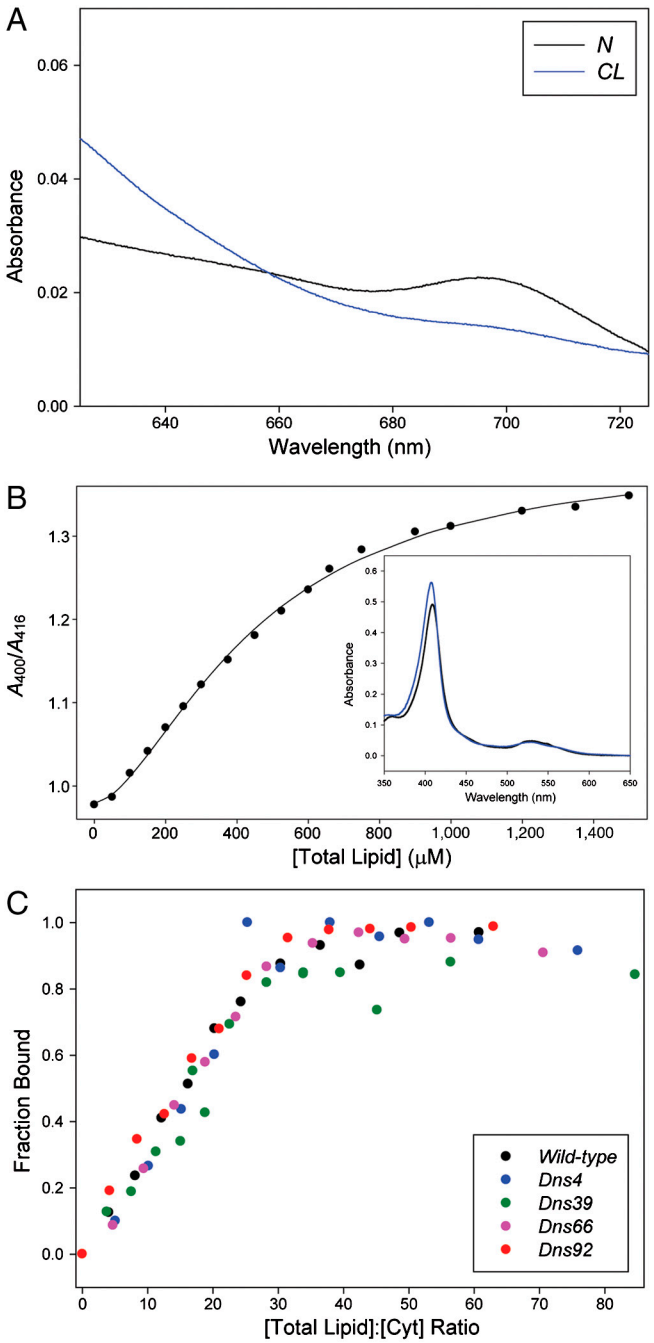

Fig. S2. (*A*) Absorption spectra showing changes in the cyt *c* S(Met-80) to Fe(III) ligand-to-metal charge transfer band in a 25 mM Hepes buffer at pH 7.4 with (CL-bound, *blue*) and without (native, *black*) TOCL/DOPC liposomes at 120-fold molar excess of total lipid to protein, ratio similar to the one used in our fluorescence experiments; ([cyt *c*] = 28 μM). (*B*) Changes in the cyt *c* Soret region as a function of total lipid concentration; ([cyt *c*] = 5 μM). *Inset*: Cyt *c* absorption spectra in a 25 mM Hepes buffer at pH 7.4 with (CL-bound, *blue*) and without (native, *black*) TOCL/DOPC liposomes at 660 μM total lipid. (*C*) Fraction of cyt *c* remaining in the supernatant after ultracentrifugation of cyt *c*-liposome solutions at various concentrations of total lipid. In these assays, TOCL/DOPC liposomes (radii $r = 50$ nm) were prepared by extrusion to ensure more uniform size distribution of vesicles and their pelleting. The protein concentrations were between 3.6 and 4.9 μM.

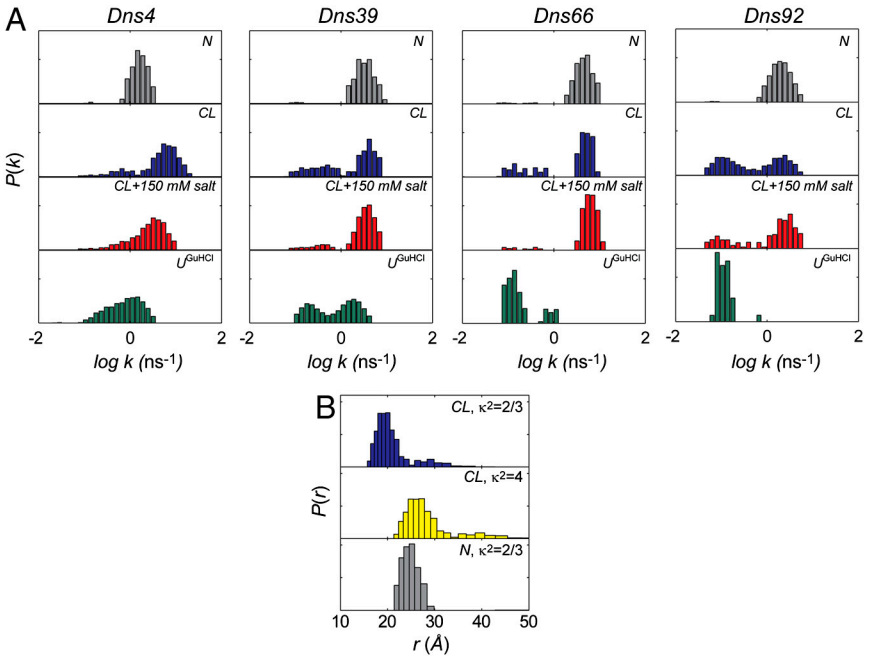

Fig. S3. (*A*) Distributions of Dns decay rates $P(k)$ of four Dns-labeled variants of cyt *c* in a 25 mM Hepes buffer at pH 7.4 [native (*N*), *gray*]; with TOCL/DOPC liposomes at 660 μM total lipid [CL-bound (*CL*), *blue*]; with TOCL/DOPC liposomes at 660 μM total lipid and 150 mM NaCl (*CL* + salt, *red*); and in 5.8 ± 0.2 M GuHCl solution at pH 7.4 [GuHCl-unfolded (U_{GuHCl}), *green*]. (*B*) Distributions of ***D*-*A*** distances $P(r)$ of Dns4 in a solution at pH 7.4 containing TOCL/DOPC liposomes at 660 μM total lipid calculated with an isotropic κ^2 value of 2/3 (*blue*) and with a maximal κ^2 value of 4 (*yellow*) as well as $P(r)$ distributions for the native protein (*gray*) in a 25 mM Hepes buffer at pH 7.4.

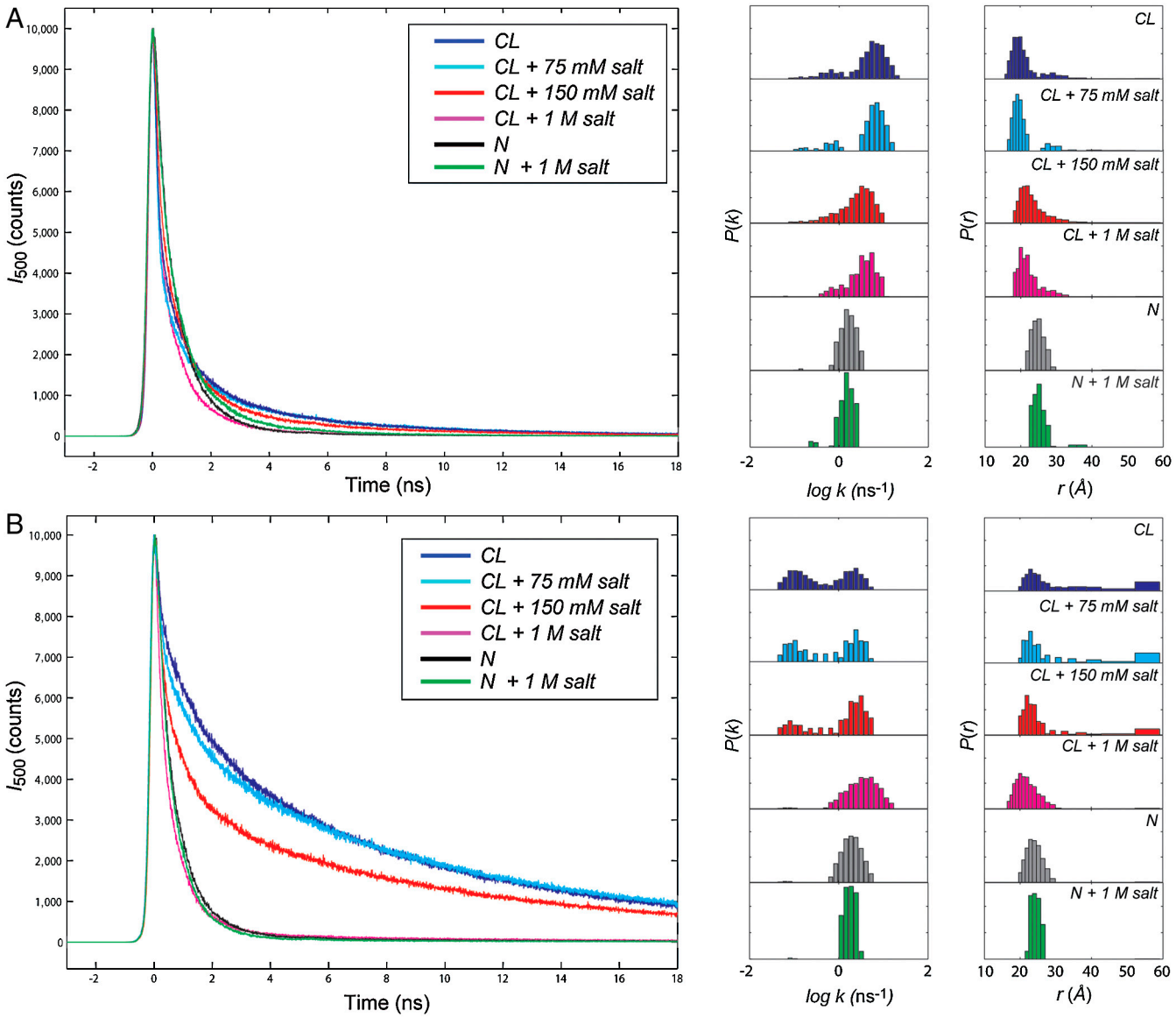

Fig. S4. TR-FRET and extracted distributions of rate constants $P(k)$ and ***D-A*** distances $P(r)$ for (*A*) Dns4 and (*B*) Dns92 in the native state (with and without added NaCl) and with TOCL/DOPC liposomes at 660 μM total lipid at indicated concentrations of NaCl.

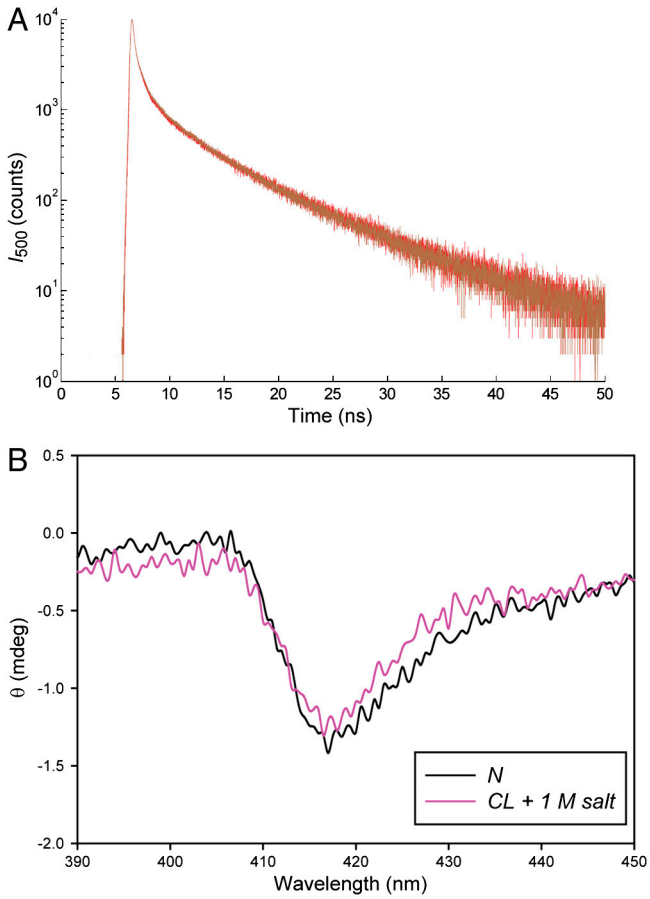

Fig. S5. (*A*) TR-FRET of Dns39 in a solution at pH 7.4 containing TOCL/DOPC liposomes at 660 μM total lipid with 150 mM NaCl added before (*red*) and after (*brown*) incubation of cyt *c* with the lipid. (*B*) Visible CD spectra of the wild-type cyt *c* in a 25 mM Hepes at pH 7.4 and 22 °C (*black*) and in a buffer solution containing 1 M NaCl and TOCL/DOPC liposomes at 660 μM total lipid (*magenta*): $[\text{cyt } c] = 5.0$ μM, $l = 1.0$ cm.

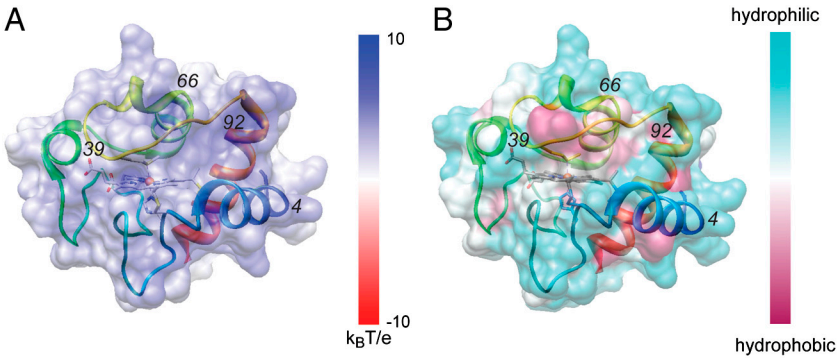

Fig. S6. (*A*) Electrostatic and (*B*) hydrophobic (the Kyte-Doolittle scale) surface maps of cyt *c* showing the positions of labeled sites. Images created with Chimera 1.5.3.

Hanske et al. www.pnas.org/cgi/doi/10.1073/pnas.1112312108

Table S1. Thermodynamic parameters for the unfolding transitions of wild-type and Dns-labeled variants of horse heart cytochrome *c

	CD[†]			Heme absorption			Dns fluorescence[‡]		
Variant	$[GuHCl]_{1/2}$, M	m_D, kJ mol^{-1} M^{-1}	$-\Delta G°f$, kJ mol^{-1}	$[GuHCl]_{1/2}$, M	m_D, kJ mol^{-1} M^{-1}	$-\Delta G°f$, kJ mol^{-1}	$[GuHCl]_{1/2}$, M	m_D, kJ mol^{-1} M^{-1}	$-\Delta G°f$, kJ mol^{-1}
Wild-type[§]	2.701 ± 0.059	11.5 ± 2.6	31.1 ± 7.1	2.595 ± 0.068	11.3 ± 2.7	29.3 ± 7.1	n.a.[¶]	n.a.[¶]	n.a.[¶]
Dns4	2.47 ± 0.11	16.6 ± 9.5	41 ± 24	2.297 ± 0.037	13.2 ± 1.8	30.3 ± 4.2	n.d.[‖]	n.d.[‖]	n.d.[‖]
Dns39	2.531 ± 0.055	17.5 ± 5.0	44 ± 13	2.31 ± 0.11	16.8 ± 9.6	39 ± 22	n.d.[‖]	n.d.[‖]	n.d.[‖]
Dns66	2.448 ± 0.057	13.8 ± 3.4	33.8 ± 8.4	2.448 ± 0.078	12.7 ± 3.7	31 ± 9	2.519 ± 0.050	13.4 ± 2.7	33.8 ± 6.8
Dns92	2.427 ± 0.028	14.1 ± 1.6	34.2 ± 3.9	2.438 ± 0.029	15.4 ± 2.1	37.5 ± 5.1	2.449 ± 0.056	19.5 ± 5.9	48± 14

*At pH 7.4 ± 0.1 and room temperature. The protein concentrations were between 7 and 11 μM.
[†]Monitored is ellipticity at 222 nm.
[‡]Steady-state measurements of fluorescence intensities.
[§]Obtained from equine heart (Sigma, C2506) and freshly purified by ion exchange chromatography.
[¶]Not applicable.
[‖]The parameter was not determined because of the poor resolution of this transition.

Table S2. Labeling sites and characteristics of the experimental distributions of donor (*D*)—acceptor (*A*) distances for dns-labeled variants of horse heart cyt *c

Labeling site	Structural unit probed	Unit's unfolding ΔG, kcal/mol)†	C^{α}-Fe distance (Å)‡§	***D-A*** Distance (Å)			Extended structures population (%)
				r^{N}_{mode} ¶	$\langle r\rangle^{RC}_{rms}$ §‖	$\langle r\rangle^{CL}_{rms}$ **	
4	*N*-helix	12.8	20	25	22	28	17
39	loop	6.0	15	22	34	25	37
66	60's helix	10	14	21	54	42††	29
92	*C*-helix	12.8	16	24	70	49††	49

*Distributions of the ***D-A*** distances $P(r)$ were extracted from analyses of the TR-FRET data.
†From NMR NHX experiments (1).
‡Calculated from the crystal structure, 1HRC (2).
§The Dns linker adds approximately 6–8 Å to this distance (3).
¶Most probable value (mode).
‖rms distance for the random-coil polypeptide calculated using the equation $\langle r\rangle_{rms} = 5.68 \times n^{0.583}$ (4). In these calculations, Cys14 was used as the heme attachment site for Dns4 and His18 was used as the heme attachment site for the other three variants.
**rms distance between the Dns fluorophore and the Fe(III) heme given by the second moment of the extracted $P(r)$ distribution.
††At distances longer than $1.5 \times R_0 = 59$ Å, energy transfer rate constants and ***D-A*** distances cannot be determined reliably; the structures with $r \geq 1.5\ R_0$ are treated as having $r = 1.5 \times R_0$ (Fig. 3) and thus experimental distributions $P(r)$ have shorter apparent $\langle r\rangle_{rms}$ values.

1 Maity H, Maity M, Englander SW (2004) How cytochrome *c* folds, and why: submolecular foldon units and their stepwise sequential stabilization. *J Mol Biol* 343:223–233.
2 Bushnell GW, Louie GV, Brayer GD (1990) High-resolution 3-dimensional structure of horse heart cytochrome *c*. *J Mol Biol* 214:585–595.
3 Pletneva EV, Gray HB, Winkler JR (2005) Many faces of the unfolded state: Conformational heterogeneity in denatured yeast cytochrome *c*. *J Mol Biol* 345:855–867.
4 Goldenberg DP (2003) Computational simulation of the statistical properties of unfolded proteins. *J Mol Biol* 326:1615–1633.

Table S3. Anisotropy parameters for Dns-labeled variants of horse heart cytochrome *c* at pH 7.4 and room temperature*

Variant	r_0†	r_∞‡	ϕ_{fast} (ns)	ϕ_{slow} (ns)	$\frac{a_{fast}}{a_{fast}+a_{slow}}$§
		folded variants			
Dns4	0.32 ± 0.01	0.028 ± 0.001	0.6 ± 0.1	2.8 ± 0.1	0.57
Dns39	0.34 ± 0.01	0.014 ± 0.001	0.2 ± 0.1	2.1 ± 0.1	0.36
Dns66	0.35 ± 0.01	0.005 ± 0.001	0.5 ± 0.1	-¶	1
Dns92	0.35 ± 0.01	0.003 ± 0.001	0.2 ± 0.1	1.6 ± 0.1	0.20
		unfolded variants‖			
Dns4	0.38 ± 0.01	0.007 ± 0.001	0.3 ± 0.1	1.3 ± 0.1	0.55
Dns39	0.39 ± 0.01	-0.001 ± 0.001	0.2 ± 0.1	1.7 ± 0.1	0.52
Dns66	0.37**	-0.002 ± 0.001	0.10 ± 0.01	4.6 ± 0.1	0.80
Dns92	0.33 ± 0.01	-0.002 ± 0.001	0.6 ± 0.1	2.9 ± 0.1	0.65
		bound to CL vesicles††			
Dns4	0.37**	0.06 ± 0.01	1.7 ± 0.1	1.9 ± 0.1	0.37
Dns39	0.37**	0.09 ± 0.01	0.8 ± 0.1	5.3 ± 0.1	0.50
Dns66	0.37**	0.09 ± 0.01	0.7 ± 0.1	4.2 ± 0.1	0.53
Dns92	0.37**	0.10 ± 0.01	0.2 ± 0.1	10.7 ± 0.1	0.51

*Analyses of the time-resolved anisotropy measurements were performed with Horiba Data Station V6 by separate treatment of the sum and difference decays.
†Apparent value of anisotropy at time equal zero.
‡The limiting value of the anisotropy decay $r(t)$ at $t = 100$ ns from fits to Eq. **S2**.
§The fraction of the anisotropy decay corresponding to the fast phase; a_{slow} and a_{fast} are the amplitudes of the two decay components from the biexponential fits of $r(t)$.
¶Attempts to include two correlation times ϕ did not result in any significant improvement of the fits; the observed value might be a composite of the global correlation time and the correlation time associated with protein segmental motions.
‖[GuHCl] = 5.8 M.
**Fixed at the known value of the Dns fundamental anisotropy (1) to improve recovery of parameters from the fits.
††With TOCL/DOPC liposomes at 660 μM total lipid in a 25 mM Hepes buffer at pH 7.4.

1 Hudson EN, Weber G (1973) Synthesis and characterization of two fluorescent sulfhydryl reagents. *Biochemistry* 12:4154–4161.